

# Cluster-subcluster mergers and the formation of narrow-angle tailed radio sources

M. Bliton,<sup>1,2\*</sup> E. Rizza,<sup>1,2</sup> J.O. Burns,<sup>1,2,3</sup> F.N. Owen,<sup>4</sup> and M.J. Ledlow<sup>1,5</sup>

<sup>1</sup> Department of Astronomy, New Mexico State University, Las Cruces, NM USA 88003

<sup>2</sup> Department of Physics & Astronomy, University of Missouri, Columbia, MO USA 65211

<sup>3</sup> Office of Research, University of Missouri, Columbia, MO USA 65211

<sup>4</sup> National Radio Astronomy Observatory †, P.O. Box O, Socorro, NM USA 87801

<sup>5</sup> Department of Physics & Astronomy, University of New Mexico, Albuquerque, NM USA 87131

Accepted 1998 May 18. Received 1998 April 15; in original form 1997 April 7

## ABSTRACT

We have examined the *ROSAT* PSPC X-ray properties of a sample of 15 Abell clusters containing 23 narrow-angle tailed (NAT) radio galaxies. We find that clusters with NATs show a significantly higher level of substructure than a similar sample of radio-quiet clusters, indicating that NAT radio sources are preferentially located in dynamically complex systems. Also, the velocity distribution of the NAT galaxies is similar to that of other cluster members; these velocities are inadequate for producing the ram pressure necessary to bend the radio jets. We therefore propose a new model for NAT formation, in which NATs are associated with dynamically complex clusters undergoing merger events. The U-shaped NAT morphology is produced in part by the merger-induced bulk motion of the ICM bending the jets.

**Key words:** galaxies:active – galaxies:clusters:general – X-rays:galaxies

## 1 INTRODUCTION

The interaction between extragalactic radio sources and the rich cluster environment in which they are often found is not well understood. Radio galaxies in the same or similar types of clusters are often found to have widely varying radio morphologies. One possible explanation for the variety of radio structures and characteristics is the “weather” within the intracluster medium (ICM). As the radio jets propagate through the hot gas, variations in the ICM density and velocity may account for the complex radio structures that are observed (Burns 1996). The interactions between radio sources and the ICM are discussed in the Burns et al. (1994a) study of radio galaxies in Abell clusters using *Einstein* IPC data. They found that 75 per cent of all radio galaxies  $>2$  arcmin in diameter have X-ray substructure within 5 arcmin of the host galaxy position, presumably due to overdense regions in the ICM. Additionally, radio galaxies tend to be more concentrated toward the centres of rich clusters, where the ICM is the densest, in comparison with the optical distribution of cluster galaxies (Ledlow & Owen 1995).

Two specific examples of the interaction between radio sources and the ICM are wide-angle tailed (WAT) and steep spectrum radio sources. WATs are radio sources located predominantly at the centre of rich clusters in D or cD galaxies, which appear to be bent by  $\approx 1000$  km s<sup>-1</sup> bulk motions of the ICM resulting from cluster-subcluster mergers (Gómez et al. 1997; Roettiger, Burns & Loken 1996). Steep spectrum sources are amorphous objects found in the centre of cooling flow clusters (Burns 1990). The cooling flow disrupts the jets (Loken et al. 1993; Burns et al. 1997), and the thermal pressure reduces the adiabatic expansion of the radio plasma. The steep spectrum is thereby produced from loss of the plasma’s high energy electrons through inverse Compton and synchrotron processes (Slee & Reynolds 1984).

Perhaps the most striking example of the interaction between the ICM and radio sources are the head-tail, or narrow-angle tailed (NAT) radio sources (O’Dea & Owen 1985). These sources have radio jets that are bent at extreme angles—up to 90° from their original orientation. The standard explanation for this radio morphology is that the jets are curved by ram pressure from the high velocity host galaxy moving through the dense ICM. This jet bending can place important constraints on both the jet dynamics and the ICM (Burns & Owen 1980). Jones & Owen (1979, JO) and Begelman, Rees & Blandford (1979, BRB) used detailed maps of the prototypical NAT galaxy NGC 1265

\* mbliton@hades.physics.missouri.edu

† The National Radio Astronomy Observatory is a facility of the U.S. National Science Foundation operated under cooperative agreement by Associated Universities, Inc.

to test models for ram pressure-induced jet bending. Numerical simulations tested the validity of these models (Balsara & Norman 1992), showing that both the JO and BRB models produce the observed NAT morphology and properties (Balsara, priv. comm.). An intriguing characteristic of narrow-angle tailed radio sources is that they have also been observed in poor clusters of galaxies (Doe et al. 1995). Such environments often have central ICM densities an order of magnitude lower than in rich clusters. Lower ICM densities require either lower radio pressures or substantially higher galaxy velocities in order to produce the ram pressure capable of bending the jets (Venkatesan et al. 1994).

A number of studies examined the relationship between NAT radio sources and the cluster environments in which they reside. Feretti, Perola & Fanti (1992) determined that NAT radio galaxies in a sample of Abell clusters appeared to be underpressured with respect to the surrounding ICM. More recently, Edge & Röttgering (1995, ER) examined the coincidence of excess X-ray emission and tailed radio sources in clusters. This research was motivated in part by the Burns et al. (1994a) result described above. Using higher resolution *ROSAT* PSPC images, ER detected compact, apparently unresolved, X-ray emission associated with NATs and concluded that this emission was caused by an AGN. However, they did not examine the relationship between the NATs and the larger-scale ICM. Specifically, does the local ICM play a role in shaping NAT galaxies, similar to the current model for WATs?

Two recent events have made this an excellent time to examine this hypothesis. First, all *ROSAT* PSPC data are now available in the public archives, and second, the completion of the 20 cm VLA Abell cluster survey (see Owen & Ledlow 1997; Ledlow & Owen 1996, and references therein) has produced a large sample of NAT galaxies in rich clusters. Together, these databases allow us to study the interaction of NAT galaxies with the rich Abell cluster environment for a representative sample of clusters.

The paper is organized as follows: In §2 we describe the samples of NAT and radio-quiet clusters used in this paper. In §3 we discuss the data analysis, including the X-ray substructure, velocity, and alignment tests. §4 contains our discussion of the results in the context of a new model for the formation of NAT radio sources. In §5 we list our conclusions. Throughout this paper, we assume  $H_0 = 75 \text{ km s}^{-1} \text{ Mpc}^{-1}$  and  $q_0 = 0.5$ .

## 2 THE SAMPLES

Two samples were utilized in this analysis: a radio-loud sample of clusters containing NATs, and a radio-quiet sample of clusters containing no detected radio sources. To define our first sample, we began with the complete, 20 cm survey of radio galaxies in Abell clusters (Ledlow & Owen 1995). This sample consists of all radio sources in Abell clusters of  $z < 0.09$  with 1.4 GHz flux density ( $S_{1.4\text{GHz}}$ )  $> 10 \text{ mJy}$  and within 0.3 Abell cluster radii ( $A_c$ ) or  $\approx 660 \text{ kpc}$ . Using the high resolution radio maps from Owen & Ledlow (1997), we examined the morphology of the radio galaxies. All radio sources showing head-tail or tadpole morphology, or resolved jets curved backward into a U-shape were classified as NATs. Questionable identifications were removed

from the sample yielding a total of 54 NATs in Abell clusters. Since the goal of this study was to examine the interaction between narrow-angle tailed radio galaxies and the ICM, we cross referenced our NAT sample with the *ROSAT* PSPC archive. We retained only clusters with X-ray images that have signal-to-noise (S/N)  $> 20$  within a 0.5 Mpc radius aperture (see §3.1 for further details on S/N), and were within the inner support ring of the PSPC. This final cut reduced the sample to 23 NAT galaxies in 15 host Abell clusters. Although the sample is no longer complete because of the requirement for pointed PSPC observations, we feel the resultant sample is representative of NAT galaxies in rich clusters. The final sample is summarized in Table 1 and X-ray/radio overlays are shown in Fig. 1.

The radio-quiet sample was also constructed from the PSPC archives. This sample includes all clusters from the VLA Abell cluster survey having no known radio sources with  $S_{1.4\text{GHz}} > 10 \text{ mJy}$ , and with redshift less than 0.09. We then chose clusters from the PSPC archives using the same criteria as the NAT clusters. We also added one cluster (A2244) at  $z=0.0968$  to increase the sample size to 13 radio-quiet clusters, which are summarized in Table 2. We chose a radio-quiet control sample (as opposed to a sample having any radio sources that were not NATs) for several reasons. Firstly, morphological classification of radio sources can be difficult and highly subjective, and although this must be done for the NAT sample, we wanted to lessen this effect as much as possible. Secondly, for the X-ray analysis, there was no longer a need to remove the contaminating X-rays from the AGN at the centres of the radio sources for our control sample. Thirdly, small, tailed radio sources may be misclassified as compact sources due to resolution limits. Lastly, the NAT morphology is only seen in low power radio sources, where the radio jets are less “stiff” and therefore more susceptible to ram pressure induced jet bending. However, higher power radio sources with stiffer jets may not display the morphological effects of ram pressure, even if it is present. In Table 3 we show a comparison of the cluster properties for the two samples. A few illustrative examples of these radio-quiet clusters are shown in Fig. 2.

In order to quantify the similarity between the two samples, we performed statistical tests on the mean and variance of the distributions of redshift, Rood-Sastry type (Rood & Sastry 1971), richness, and X-ray luminosity. First, we used the Student’s T-statistic (Havlicek & Crain 1988) to compare the mean of each distribution. This statistic tests the validity of the null hypothesis that the two distributions have the same mean. Values of significance  $< 5$  per cent require one to reject the null hypothesis. The significance levels for this test are shown in Table 3; note all significance levels are above 5 per cent. We used the F-test (Havlicek & Crain 1988) to determine if the distributions have significantly different variances in the cluster parameters. Similar to the Student’s T-statistic, the F-test examines the null hypothesis that the two samples have the same variance. The significance values for this test (Table 3) again show that for most cluster properties, the null hypothesis cannot be rejected. The one exception is in X-ray luminosity where the variances of the two samples are similar at only the 3 per cent level. However, since the mean luminosities are not significantly different and all other cluster proper-

**Table 1.** NAT cluster properties

Abell #	IAU Name	Cluster $z^a$	ROR #	Exposure (s)	Rood–Sastry	Richness class <sup>b</sup> (#) <sup>c</sup>	$\sigma_v^a$ (km s <sup>-1</sup> )
85	0039-095A 0039-097	0.0556	800250	10240	cD	1(59)	749
119	0053-015 0053-016	0.0444	800251	14700	C	1(69)	778
194	0123-016A	0.0180	800316	24500	L	0(37)	440
496	0431-134	0.0327	800024	8600	cD	1(50)	741
514	0445-205 0446-205	0.0734	800278	17500	F	1(78)	
754	0906-095	0.0534	800232	6200	cD	2(92)	1048
1314	1131+493 1132+492	0.0338	800392	2800	C	0(44)	664
1367	1142+198 1141+202B	0.0214	800153	18100	F	2(117)	822
1656	1256+281	0.0231	800005	20400	B	2(106)	880
1775	1339+266B	0.0724	701068	12900	B	2(92)	1594
1795	1346+268B	0.0622	800055	25000	cD	2(115)	896
2142	1556+274	0.0896	800233	4800	B	2(89)	1241
2255	1712+640 1712+641	0.0808	800512	14600	C	2(102)	1221
2256	1705+786 1706+786 1706+787	0.0581	100110	16600	B	2(88)	1270
2589	2321+164	0.0416	800526	7100	cD	0(40)	500

<sup>a</sup> Struble & Rood (1991)

<sup>b</sup> Abell, Corwin & Olowin (1989)

<sup>c</sup> Number of cluster members (Abell, Corwin & Olowin 1989)

**Table 2.** Radio-quiet sample properties

Abell #	Cluster $z^a$	ROR #	Exposure (s)	Rood–Sastry	Richness class <sup>b</sup> (#) <sup>c</sup>	$\sigma_v^a$ (kms <sup>-1</sup> )
539	0.0291	800255	9600	F	1(50)	701
548	0.0414	800041	3800	F	1(79)	872
644	0.0704	800379	11200	cD	0(42)	
744	0.0729	700385	6100	B	0(42)	812
1139	0.0383	701198	4320	I	0(39)	
1377	0.0514	800106	4900	B	1(59)	488
1651	0.0845	800353	10600	cD	1(70)	965
1691	0.0722	800295	10600	cD	1(64)	
1750	0.0855	800553	23400	F	0(40)	778
1837	0.0376	800243	15700	cD	1(50)	218 <sup>d</sup>
2107	0.0421	800509	8300	cD	1(51)	536
2244	0.0968	800265	2965	cD	2(89)	1240
2670	0.0761	800420	54700	cD	3(142)	881

<sup>a</sup> Struble & Rood (1991)

<sup>b</sup> Abell, Corwin & Olowin (1989)

<sup>c</sup> Number of cluster members (Abell, Corwin & Olowin 1989)

<sup>d</sup> Zabludoff et al. 1993

ties are similar, we feel that these samples are adequate for comparison.

### 3 DATA ANALYSIS

The X-ray analysis used the PSPC hard-band (0.4–2.4 keV) count maps and exposure maps from the *ROSAT* archive at the Goddard Space Flight Center. Average background values for the sample were determined within the inner support

ring of the PSPC and subtracted from the count maps. The only exceptions were A754, A1367, and A1656, where the cluster emission itself completely filled the inner ring region. The count maps were divided by the exposure maps to produce surface brightness images in units of counts s<sup>-1</sup> pixel<sup>-1</sup>, where each pixel is 15 × 15 arcsec<sup>2</sup>. All X-ray data were smoothed with a 45 arcsec FWHM (32.6 kpc for  $z=0.04$ ) Gaussian filter. The AIPS software package was used for aligning and resizing the images as well as producing over-

**Table 3.** Comparison of samples

Cluster property	Mean			Variance <sup>a</sup>		
	NAT	RQ	Sig. per cent	NAT	RQ	Sig. per cent
$z$	0.051	0.062	22	0.00055	0.00053	98
Rood-Sastry type	2.3	2.6	71	2.0	4.1	19
Richness #	79	64	18	740	881	75
X-ray luminosity ( $\times 10^{44}$ )	1.5	1.0	44	4.9	1.3	3

<sup>a</sup>The variances of redshift and richness seem extremely high due to the effects of having flat distributions (i.e. large  $\sigma$ ), and that the means are significantly different from unity. This causes the variances ( $\sigma^2$ ) to appear very large or very small.

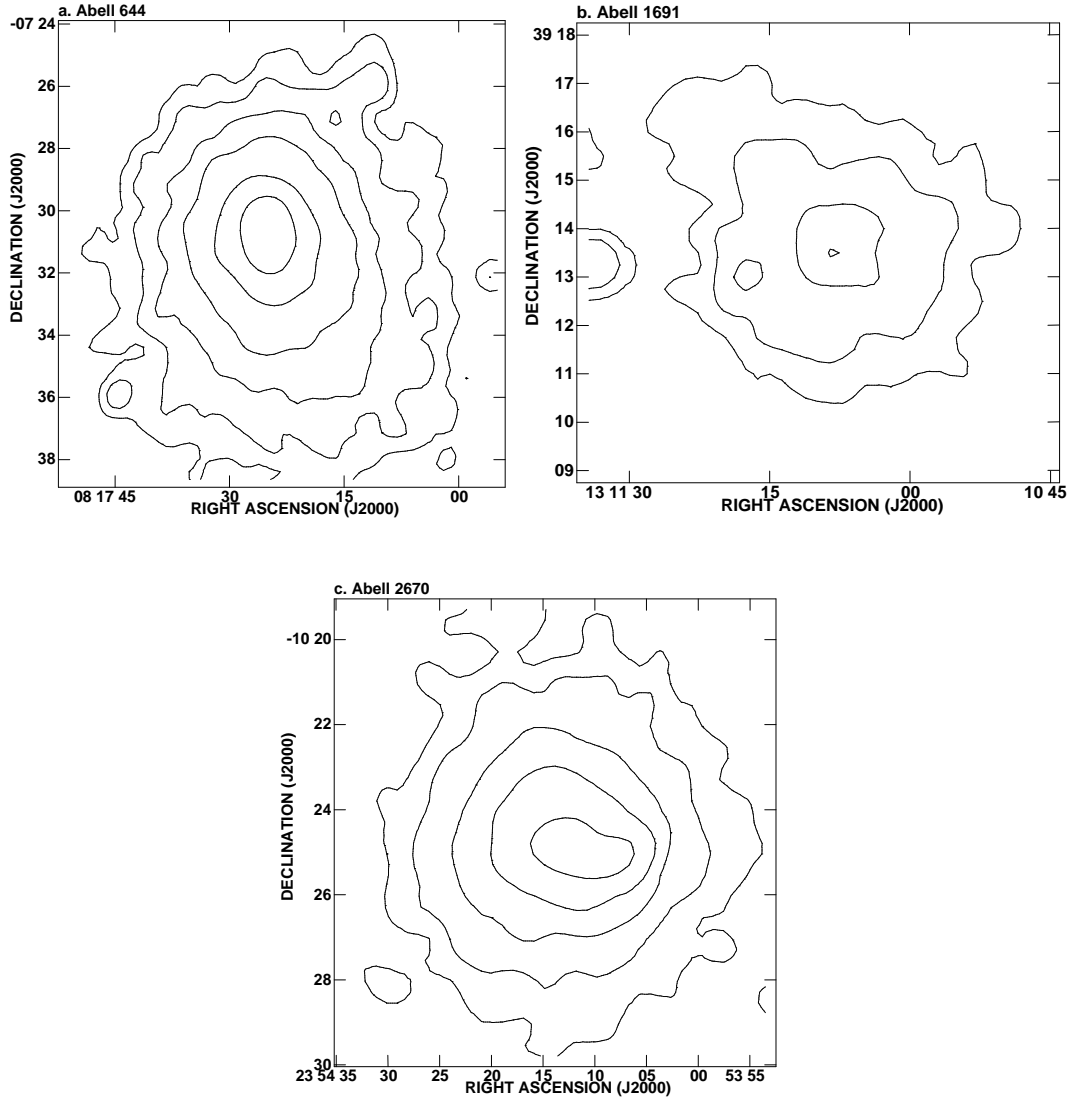


**Figure 1.** ROSAT PSPC X-ray surface brightness contours of three radio quiet clusters, (a) Abell 644, (b) Abell 1691, and (c) Abell 2670. For all maps, X-ray surface brightness contours are at  $3\sigma$ ,  $5\sigma$ ,  $10\sigma$ ,  $20\sigma$ ,  $50\sigma$ , &  $100\sigma$ .

lays of the radio/X-ray images. In Fig. 1, we show radio greyscale overlaid on to X-ray surface brightness contours for the NAT sample. Comments on individual clusters and NATs are given in the Appendix (§6).

The luminosity for each cluster was determined by extracting a circular region of diameter 0.5 Mpc, centred on the peak of the X-ray emission. The extracted region was modeled with the best-fitting Raymond & Smith thermal plasma model (Raymond & Smith 1977), with 30 per cent solar metal abundance, using the XSPEC X-ray spectral fitting software. This model was then used to compute the 0.4–2.4 keV X-ray luminosity for each cluster.

### 3.1 Substructure

For a fully virialized cluster gravitational potential, one would expect to observe a smoothly varying X-ray surface brightness profile. However, this is not what we see in many of the NAT clusters (Fig. 1). For example, Abell 85 (Fig. 1a) possesses a clear elongation to the south with a clump of extended emission in the vicinity of a NAT. Abell 514 (Fig. 1e) and Abell 1314 (Fig. 1h) exhibit clumpy, elongated, and highly non-circular X-ray structures. The X-ray peak of Abell 754 (Fig. 1g) is markedly offset from the centre of the X-ray emission. These clear examples of cluster substructure manifest themselves in significant radial variations of the centroid ( $R_o$ ) of the X-ray image. Mohr, Fabricant & Geller (1993) have argued that a centroid shift in the X-ray surface brightness profile of a cluster is a robust measure of substructure. Since the X-ray surface brightness distribution of a cluster is a direct measure of the ICM density distribution, a centroid shift in X-ray emission indicates a non-smooth density distribution, which in turn indicates a dynamically complex cluster. This direct link between centroid shift and a cluster’s dynamical state makes this test a strong measure of cluster substructure.

In an effort to quantify cluster substructure, elliptical isophotes were fit to the X-ray maps using the IRAF STSDAS task ELLIPSE, based on the algorithm by Jedrzejewski (1987). The initial centroid was set to the X-ray peak of the cluster emission, and all contaminating point sources were masked out. The ELLIPSE task performs an iterative fit to the emission weighted centroid of the X-ray distribution as a function of semimajor axis,  $a$ . To increase the signal-to-noise, we used smoothed images for the isophotal fits. We therefore kept the step in semimajor axis,  $a$ , to be at least 1.5 pixels ( $2a = 45$  arcsec) in order to avoid correlated errors in adjacent radial bins.

The ELLIPSE task produces a radial profile of  $x$  and  $y$  (RA & Dec.) centroid coordinates. These two components were converted into a radial vector,  $R_o$ , at each bin. For each cluster, the radial profiles were further divided into two portions—one region from the cluster centre to a semimajor axis of 150 kpc, and a second region from 150 to 300 kpc. The values of  $R_o$  were averaged for the two regions, and these two average values were differenced to obtain  $\Delta R_o$ . To illustrate this process we show the radial variation of  $R_o$  for clusters with large (A754) and small (A1837) centroid shifts in Fig. 3.

Histograms showing the distributions of  $\Delta R_o$  for both the NAT and radio-quiet cluster samples are shown in Fig. 4. Examination of the figures show that NAT clusters ex-

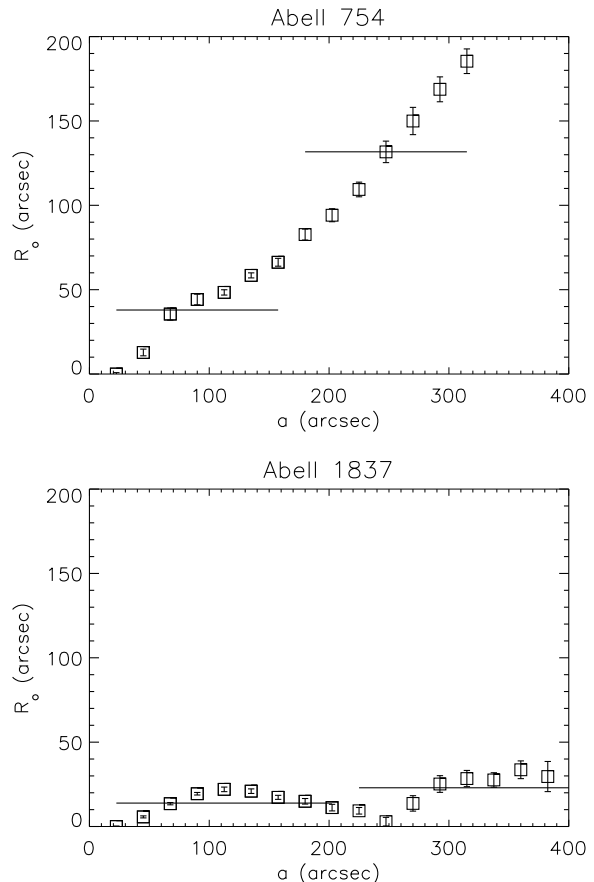


**Figure 2.** Radial variation of  $R_o$  for (a) Abell 754 and (b) Abell 1837. The horizontal lines mark the regions 0–150 kpc, and 150–300 kpc.

hibit preferentially larger values of  $\Delta R_o$  than the radio-quiet clusters. To determine the statistical significance of this difference, the student’s T-test was performed. The means of the  $\Delta R_o$  distributions revealed the samples to be similar at a 0.3 per cent level of significance, indicating that the two distributions have significantly different means. A similar result is obtained when using the Kolmogrov–Smirnov (KS) test (1.7 per cent significance level), which is sensitive to the shapes of the distributions.

While performing this analysis, we were concerned about the use of the ELLIPSE routine in IRAF to determine the centroid shift. Are the solutions generated by ELLIPSE stable, and how large are the errors associated with this task? Do the errors depend on the signal-to-noise of the data? We have attempted to answer these questions by generating errors for the centroid shifts using a bootstrap resampling algorithm. First, we generated 1000 realizations of every cluster count map by reassigning values to each pixel based on the Poisson probability distribution, with the original pixel value as the mean of that distribution. Therefore, each resampled pixel could have a large range of possible values, but was most likely to have the value of the original data. We then ran the identical ELLIPSE task on all 1000 realizations, giving us a range of centroid shifts. From this distribution of  $\Delta R_o$ , we used the best-fitting Gaussian function to determine the mean and standard deviation of

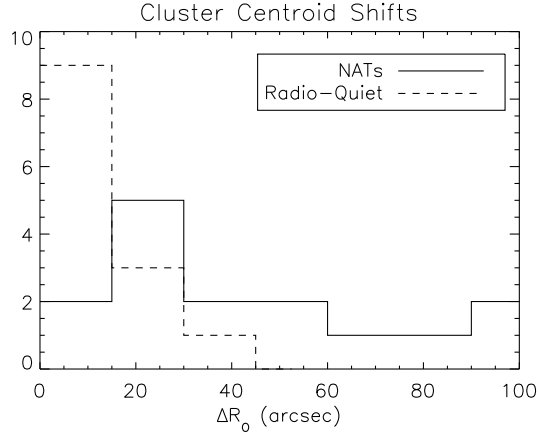


**Figure 3.** Histograms of  $\Delta R_0$  values for the NAT and radio-quiet samples. The NAT sample shows a significantly broader distribution of  $\Delta R_0$  values than the radio-quiet clusters.

the centroid shift for each cluster, which are shown in Table 4. As expected, the largest standard deviations occur in clusters with the lowest S/N. The smallest generally occur in clusters possessing strong cooling flows, where the S/N is high, and the core substructure low.

To quantify whether the two distributions were significantly different given the bootstrap errors, we calculated the means of the  $\Delta R_0$  values for each sample, weighting the means by their standard deviations. We also computed the errors on the means from the individual errors on  $\Delta R_0$ . The means of the two distributions, shown at the bottom of Table 4, differ by  $3.6\sigma$ , yielding a probability of  $>99.9$  per cent that the two distributions have different means. Therefore, we again conclude that clusters containing NATs show a higher degree of substructure than similar radio-quiet clusters.

### 3.2 Velocities

The X-ray substructure result above implies that these clusters are in an interesting, non-relaxed state. To pursue this further, we examined the dynamics of the NATs with respect to the rest of the cluster galaxies. Radio sources in general tend to have low peculiar velocities compared to other cluster members (Owen, Ledlow & Keel 1995), yet in the standard model for narrow-angle tailed radio source formation, NATs should be associated with high velocity galaxies. Large peculiar motions of NAT galaxies are required to produce the ram pressure necessary to bend the radio tails into the observed **U** shapes.

For this velocity analysis, we returned to the complete sample of 54 NATs. In order to compare galaxies in different clusters, all galaxy velocities were normalized to their cluster’s velocity dispersion, by using the parameter  $U = (v_o - v_c)/\sigma$ , where  $v_o$  is the galaxy velocity,  $v_c$  is the mean cluster velocity, and  $\sigma$  is the cluster velocity dispersion (Owen et al. 1995). The NATs in the sample were compared to radio-quiet cluster galaxies as well as other radio sources. The general radio source sample consisted of all radio galaxies, excluding NATs, in the Ledlow & Owen (1995) sample for which there were velocity data available (Owen

et al. 1995). Since the NATs were removed from this sample, most of these radio sources were morphologically linear, and not sharply bent. These sources are expected to have velocities significantly lower than NAT galaxies, if the standard model for NAT formation is correct. Since  $\sigma$  must be used in this analysis, only NATs in clusters with published velocity dispersions were included, reducing the sample size to 31. To simulate typical cluster galaxies, we generated a Gaussian distribution of velocities using Monte Carlo sampling. The simulated distribution was compared with the NAT sample, as well as the other radio sources, to check the similarity of the distributions. A histogram comparing the three distributions is shown in Fig. 5.

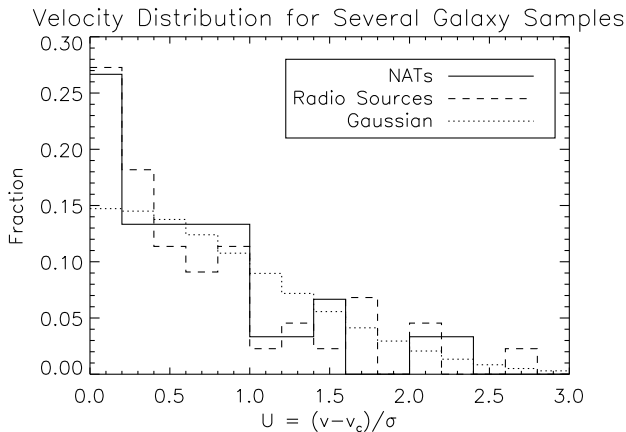
Using the student’s T-test, we find the mean of the NAT galaxy distribution is statistically similar to both the simulated cluster galaxies and the other radio sources. This result is contrary to the standard model of NAT formation, which requires the host galaxy to have a large peculiar motion ( $\sim 1000 \text{ km s}^{-1}$ ) in order to produce the ram pressure necessary to bend the radio jets. One would therefore expect a much broader distribution in  $U$  (typical  $U \approx 1.0$ ) for NAT galaxies compared to other radio sources. The observed distribution of NAT velocities is clearly incapable of producing the needed ram pressure for jet bending.

There is a potential projection effect which could skew the above analysis. In order to classify radio galaxies as NATs, the tails must be projected away from the observer’s line of sight. Any NAT with its radio tail parallel to the line-of-sight will not be classified as a NAT. If the direction of NAT tails is due primarily to the motion of the host galaxy, then the NATs with the highest line-of-sight velocities will not be included in this analysis. Therefore, the observed NAT distribution may be peaked toward low velocities by excluding objects with high line-of-sight velocities. We attempted to determine the magnitude of this effect by calculating the change in an expected distribution of NAT velocities once galaxies moving parallel to the line-of-sight are removed. For our idealized distribution of NATs, we produced a Gaussian 3D velocity distribution centred at  $1000 \text{ km s}^{-1}$  larger than a cluster’s central velocity. This is chosen since velocities on the order of  $1000 \text{ km s}^{-1}$  are considered necessary for jet bending (O’Dea 1985; Eilek et al. 1984). The Gaussian distribution had a  $\sigma = 400 \text{ km s}^{-1}$ , in order to leave only 10 per cent of the total number of NATs with velocities less than  $500 \text{ km s}^{-1}$ . We then gave the NATs random projection angles distributed uniformly about the sky, and calculated the NATs’ line-of-sight velocity distribution from their 3D velocities and their projection angles.

To simulate the effects of not detecting NATs with their radio tails pointing toward the observer, we removed all galaxies with 1-D velocities  $< 45^\circ$  from the line-of-sight. This distribution was converted to  $U$  as described above, and compared to the observed NAT velocity distribution (Fig. 6). Using the student’s T-test, we find that the observed NAT distribution and the simulated NAT distribution have significantly different means. Clearly, projection effects cannot account for the observed NAT distribution. Therefore, our conclusion stands that NATs have velocities incapable of bending their radio jets via ram pressure.

**Table 4.** Results of bootstrap analysis

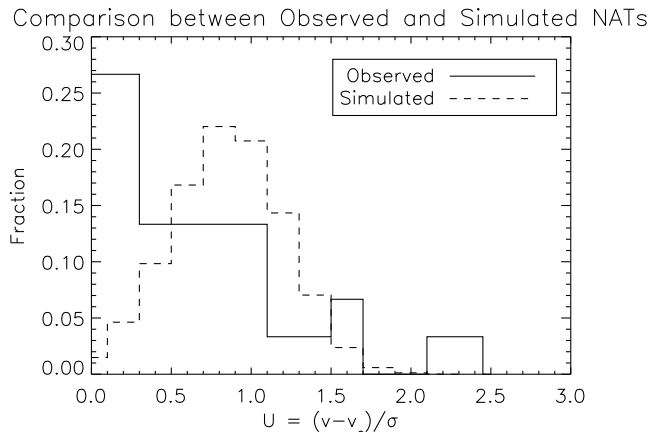
NAT Clusters				Radio-quiet Clusters			
Abell #	$\Delta R_{\text{actual}}$ (arcsec)	$\Delta R_{\text{centre}}$ (arcsec)	$\sigma_{\Delta R}$	Abell #	$\Delta R_{\text{actual}}$ (arcsec)	$\Delta R_{\text{centre}}$ (arcsec)	$\sigma_{\Delta R}$
85	24	24	1.8	539	11	12	6.8
119	15	11	15.6	548	2	27	35.5
194	19	13	43.7	644	24	24	2.2
496	28	28	3.2	744	8	11	7.7
514	52	54	11.5	1139	36	40	22.2
754	94	93	11.4	1377	20	27	15.0
1314	42	49	28.3	1651	6	7	1.8
1367	61	55	25.6	1691	5	3	5.4
1656	93	93	6.2	1750	7	8	3.8
1775	32	32	4.1	1837	9	10	7.2
1795	16	16	1.0	2107	6	6	4.1
2142	3	3	1.1	2244	4	4	2.4
2255	57	59	6.1	2670	18	17	3.7
2256	90	89	4.8				
2589	5	7	3.3				
	Mean: 16				Mean: 11		
	$\sigma_{\text{mean}}: 0.6$				$\sigma_{\text{mean}}: 1.0$		


**Figure 4.** The velocity distributions for the sample of NATs, all other radio sources, and a simulated Gaussian galaxy cluster velocity distribution.

### 3.3 Radio tail orientation

In an effort to understand the orbits of NAT galaxies, O’Dea, Sarazin, & Owen (1987) examined the directions of NAT tails with respect to the Abell cluster centres. Assuming the NAT tails are indicators of the direction of motion of the host galaxies, the resulting random orientation led them to suggest that the overall distribution of NATs is consistent with isotropic galaxy orbits. However, only considering NATs located within 0.5 Mpc, the galaxies exhibited a trend towards radial orbits.

We performed the same analysis as O’Dea et al. (1987) for our NAT sample with a slight modification. This modification was motivated by the fact that a number of the NAT sources possess bent or curved tails, leading to ambiguity in determining a single position angle (e.g. NATs in Abell 514 and Abell 2255). We therefore defined two radio position angles:  $\theta_I$ —the angle formed by a line from the head of the radio emission to the point at which the tail bends,


**Figure 5.** The velocity distributions for the observed NAT sample and the simulated NAT sample. The simulated sample does not include NATs with velocity vectors  $< 45^\circ$  from the line-of-sight.

and  $\theta_F$ —the angle formed by a line from the point at which the tail bends to the  $3\sigma$  end of the radio tail. For the NAT sources which did not show significant bending, the overall tail direction was used for both  $\theta_I$  and  $\theta_F$ .

$\theta_I$  and  $\theta_F$  were subtracted from the position angle of the radial vector drawn from the NAT to the Abell cluster centre, yielding  $\Delta\theta_I$  and  $\Delta\theta_F$ . The relatively flat distribution in  $\Delta\theta$  appears consistent with random tail orientations (Fig. 7). To test the statistical significance of this hypothesis, we compared the two samples with a theoretical, random distribution using the KS test. For  $\Delta\theta_I$ , the datasets are drawn from the same distribution at the 91.4 per cent confidence level. For  $\Delta\theta_F$ , the datasets are drawn from the same distribution at the 59.9 per cent confidence level. We therefore see no indication that this NAT sample deviates from a random orientation relative to the optical Abell cluster centre.

Using the same initial and final position angles as above, we compared the tail orientations to a line between the NAT

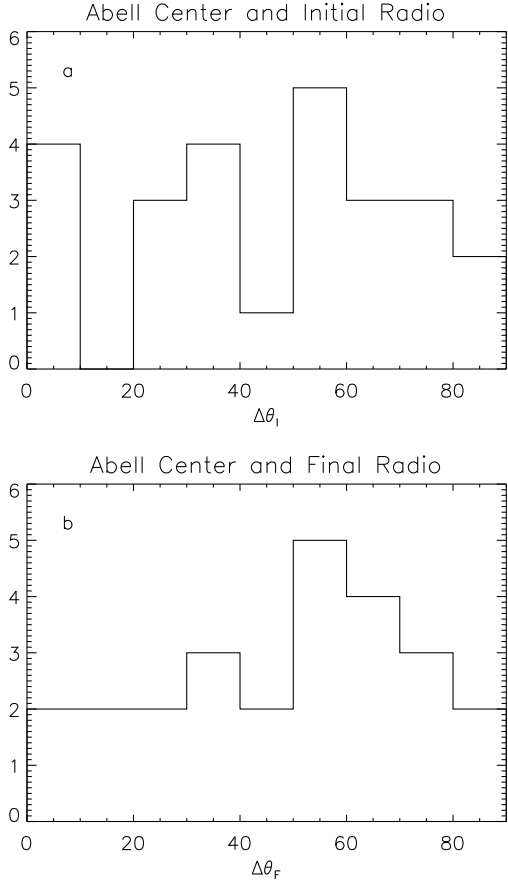


**Figure 6.** The angle between the NAT tails and the line connecting the NAT to the Abell cluster centre for both the (a) initial tail direction and the (b) final tail direction. Both distributions are consistent with an isotropic distribution of NAT tails.

and the peak of the cluster X-ray emission. This was done under the assumption that the X-ray peak may give a better indication of the centre of the cluster potential well. The  $\Delta\theta_I$  and  $\Delta\theta_F$  distributions for this analysis are shown in Fig. 8. The KS test was applied yielding significance levels of 74 per cent for  $\Delta\theta_I$  and 84 per cent for  $\Delta\theta_F$  with respect to a random distribution. Again, the directions of the NAT tails are consistent with random orientations in clusters.

### 3.4 Radio tails and X-ray substructure

Although we found no correlation between the radio tails and the X-ray/optical cluster centres, there is a potential alignment between the radio tails and X-ray cluster elongations (see e.g. A119, A1656, and A2142 in Fig. 1). To quantify this potential result, we examined the orientations of the radio tails with respect to the regions of X-ray excess or elongation. We defined two X-ray position angles:  $\theta_{\text{local}}$ —the position angle of an X-ray enhancement located within 1 arcmin of a NAT radio source, and  $\theta_{\text{global}}$ —the position angle of the entire X-ray emitting cluster.

To measure these position angles we needed to determine regions of significant excess throughout the entire cluster. Due to the rapid fall-off of surface brightness with distance from the cluster centre, the isophotal variation analy-

sis described in §3.1 is only sensitive in the inner  $\sim 8$  arcmin (450 kpc for  $z=0.05$ ) of the clusters. Therefore, in order to probe excess emission in the outer regions of the cluster, as well as global cluster elongations, we used an alternative probe for substructure detailed in Gómez et al. (1997). We fit circular models to the cluster emission and subtracted them from the parent map. We specifically chose circular models to increase our sensitivity to elongation in the overall cluster emission. The residual maps were examined for regions of excess within 1 arcmin of a NAT radio position, and these excess regions were tested for significance using Poisson statistics. For each region of interest, the number of counts in the cluster image was compared to a similar region in the model image. The summed probability of obtaining the number of observed counts above the model value was calculated, and any region of 99 per cent significance or higher was considered to be substructure. The regions of excess were used to calculate the position angle of the local substructure,  $\theta_{\text{local}}$ . The global position angle was determined at the radius where the X-ray emission fell to approximately  $5\sigma$  above the background.

We examined the correlation between each of the four possible radio-X-ray position angles by measuring the difference between the NAT and cluster orientations. These distributions (shown in Fig. 9) were compared with a theoretical, random distribution similar to the analysis described in §3.4. None of the distributions deviated significantly from a random distribution.

### 3.5 Compact X-ray emission near NATs

ER examined compact X-ray emission coincident with narrow-angle tailed radio sources. They found all such emission to be unresolved and found a correlation between the X-ray flux and the core radio flux density. This led them to conclude that the X-ray emission associated with NATs is most likely due to the AGN at the centres of the galaxies. We performed a similar analysis for our slightly different sample of NAT galaxies. To best probe the X-ray emission associated with the NATs, we subtracted an elliptical model of the overall cluster emission from each image using the method described in §3.1. The residual maps were examined for remaining compact X-ray emission near the NAT radio sources. X-ray detections with centroid positions located more than 1.5 arcmin from the published centres of the radio sources were discarded. This left 40 per cent ( $\frac{10}{25}$ ) of the NATs with coincident, compact X-ray emission. Radial profiles were extracted from these regions in order to determine their extents. Since the PSPC point spread function (PSF) is highly energy dependent, the spectral information for these sources was needed. Thus we extracted X-ray spectra for the regions using the PROS task QPSPEC and calculated the energy dependent PSF using the FTOOLS task PCRPSF. The model of the PSF was compared to the extracted radial profiles of the compact emission using the  $\chi^2$  statistic. In agreement with the ER result, none of the detected sources appear to be significantly resolved.

Only one NAT in our sample (3C264 in Abell 1367) had sufficient counts to perform an adequate spectral fit to the X-ray emission. The spectral distribution was rebinned, so that all spectral channels had at least 25 counts ( $S/N \sim 5$ ). Using the XSPEC software package, we fit the spectrum separately



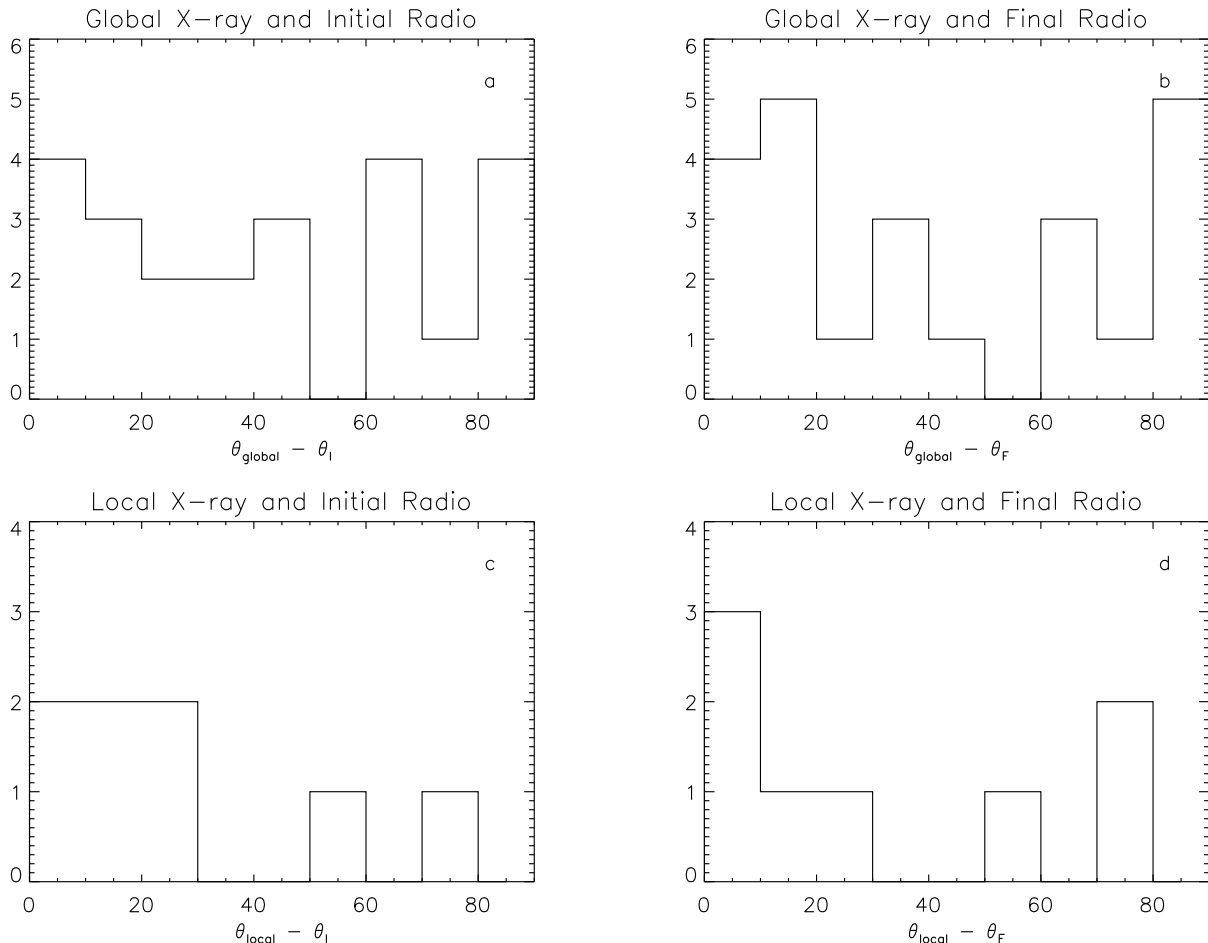


**Figure 8.** The difference between the various radio and X-ray position angles, as described in the paper, folded into  $90^\circ$ .

with a power-law and a Raymond & Smith thermal model, to attempt to determine whether the X-ray emission was due to an AGN or the galaxy ISM. Similar to the ER result, the spectral fits were inconclusive, giving equally good statistics for both models. Using *ASCA*, Forman (priv. comm.) also found 3C264 to be well fit with either a 3 keV thermal model (the same temperature as the surrounding emission) or a power-law.

The correlation between the core radio and the X-ray flux density noted by ER, led them to suggest another constraint on unification schemes between FR I radio sources and BL Lac objects. We performed a similar analysis for our sample, computing the X-ray and radio fluxes. The X-ray emission was modeled as an absorbed power-law with energy index 2.4 as done by ER. The X-ray fluxes for all sources, including upper limits on non-detections, are given in Table 5. The luminosities are also listed in Table 5 as well as limits on the linear diameter of unresolved sources based on the approximate spatial resolution of the PSPC. Also included in the table are the 1.4 GHz core radio power for the NATs. Whenever possible, the radio powers were taken from O’Dea & Owen (1985). If the radio powers were not available we measured them from the maps of the VLA Abell cluster survey using AIPS. The X-ray luminosities and the core radio powers for all 23 NATs are plotted in Fig. 10.

Since more than half the NATs (57 per cent) only have upper limits on the X-ray flux, we used the survival analysis routines available in the ASURV software package Rev 1.1 (La Valley, Isobe, & Feigelson 1992), which implements the methods presented in Isobe, Feigelson, & Nelson (1986), to search for a correlation between core radio power and X-ray luminosity. Using the generalized Kendall’s  $\tau$  correlation test, we find the probability for no correlation is 5.4 per cent, so although the data are suggestive of a correlation, we cannot reject the null hypothesis. With the current data, it is impossible to determine the origin of the X-ray emission from NATs.

If the X-ray emission does not arise from an AGN, then what is its origin? One possibility is the galaxy ISM. The JO model of NATs proposes that there is an inner ISM with radius 4–50 kpc, not stripped by ram pressure. This gas is expected to have  $T \sim 1$  keV (reflective of the stellar velocity dispersion) and X-ray emission comparable to that observed in other ellipticals. Simulations of an elliptical galaxy moving through the ICM (Balsara, Livio, & O’Dea 1994) show that the outer galaxy ISM is strongly affected by ram pressure stripping, producing shocks which propagate into the galaxy core and which may also heat the ISM. The current limit on the sizes of the compact X-ray emission regions and the observed X-ray luminosities (see Table 5) are consistent

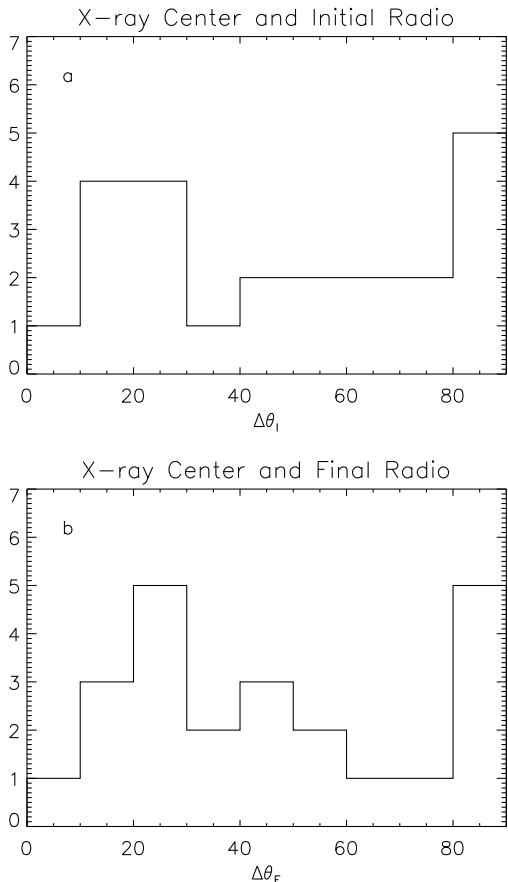


**Figure 7.** The angle between the NAT tails and the line connecting the NAT to the cluster X-ray peak for both the (a) initial tail direction and the (b) final tail direction. Both distributions are consistent with an isotropic distribution of NAT tails.

with this model and with observations of other ellipticals (Fabbiano 1989). Higher resolution HRI X-ray observations of three NATs are currently underway which should help us to discriminate between AGN and ISM models.

#### 4 NAT FORMATION THROUGH CLUSTER-SUBCLUSTER MERGERS

The current paradigm for NAT formation fails to account for the new observed properties of NAT galaxies in rich clusters presented in this paper. The canonical view of NAT radio sources assumes the host galaxies are moving at transonic velocities (i.e. 1–2 times the velocity dispersion) through the dense ICM of spherical, relaxed clusters. In this picture the galaxy velocity and ICM density provide the ram pressure necessary to bend the radio jets. However, this model does not account for the fact that NATs are preferentially found in dynamically complex, possibly evolving clusters with significant X-ray substructure. Additionally, if the NAT tails are bent from ram pressure by high velocity galaxies, then these radio sources should show high peculiar motions. However, NATs tend to have, on average, velocities similar to a typical cluster galaxy.

We therefore propose a new model for NAT formation,

in which NATs are associated with dynamically complex clusters undergoing merger events. Using an N-body + Hydro code, detailed simulations of merging clusters have been performed (Roettiger, Burns & Loken 1993, 1996; Schindler & Müller 1993). One signature of merging is bulk flows in the cluster gas with velocities  $> 1000 \text{ km s}^{-1}$  aligned with the X-ray elongation. The resulting ram pressure of these ICM bulk flows is sufficient to sweep back the radio jets (e.g. Loken et al. 1995). This ram pressure from the cluster gas would explain why these radio sources, which tend to have typical cluster velocities, exhibit the NAT radio morphology. This is similar to our model for the formation of wide-angle tailed radio sources (Gomez et al. 1997), which also possess bent tails due to the motion of the ICM. However, since NAT radio sources tend to have lower radio powers (and possibly lower jet momentum fluxes) than their WAT counterparts (O’Donoghue, Eilek & Owen 1993), this may explain why NAT jets are bent to larger angles.

The ICM bulk motion may explain several other NAT observations as well. Numerical simulations of an elliptical galaxy moving supersonically through the ICM (Balsara et al. 1994) show compression of the ISM, with shock formation inside the galaxy, near the core. Since free-free emission is proportional to the square of the gas density, a small change in density produces a larger change in the luminosity. This may cause the gas in some NAT galaxies to become detectable in the X-ray, and may explain the high fraction of NAT galaxies (40 per cent) with unresolved X-ray emission. Additionally, the luminosities and sizes of the of the observed X-ray emission from NATs (Table 5) is consistent with this model.

A second result of the Balsara, Livio, & O’Dea simulation is the periodic inflow of gas from the downstream side of the galaxy into the galaxy core (inner  $\sim 1 \text{ kpc}$ ), similar to the accretion of stellar winds on to compact objects (Ishii et al. 1993; Ruffert & Arnett 1994). Although the resolution of the simulation is not high enough to determine the fate of the gas at the core, some fraction of it could fall on to the accretion disc. This process could in turn feed the central engine and increase the radio luminosity. These mechanisms for enhanced radio and X-ray emission from NATs are an alternative explanation for the correlation between core radio power and X-ray luminosity discussed in §3.5.

Another common feature of NAT galaxies is the exceedingly long (up to 1 Mpc) radio tails (e.g. IC 711 in A1314, Vallée & Wilson 1976). It is difficult to understand how the relativistic particles can travel and then radiate at these distances from the cores (Ekers et al. 1978; Wilson & Vallée 1977; Simon 1979; Vallée & Roger 1987). Clearly, there must be a substantial particle reacceleration mechanism. But where does the energy come from to power the in-situ particle acceleration? The kinetic energy of the ICM from cluster-subcluster mergers could provide the energy input necessary for this reacceleration.

This new model for NAT formation is able to produce the morphology of these unique radio sources. In addition, it is able to account for the X-ray substructure and velocity results presented in this paper, and may explain the other NAT characteristics described above. Therefore, we conclude that this new process for NAT formation provides important insight into the cluster environment in which NATs reside. Since NATs are preferentially formed in merging clus-

**Table 5.** NAT galaxy properties

Abell #	IAU Name	X-ray Flux $10^{-14}$ ergs $\text{cm}^{-2}$ $\text{s}^{-1}$	X-ray Luminosity $10^{41}$ ergs $\text{s}^{-1}$	Core Radio Power <sup>a</sup> $10^{23}$ W $\text{Hz}^{-1}$ at 1.4 GHz	X-ray Diameter kpc
85	0039-095A	< 6.8	< 1.9	0.20	29
	0039-097	$9.8 \pm 1.5$	$5.3 \pm 0.8$	0.40	
119	0053-015	$3.0 \pm 0.7$	$1.0 \pm 0.3$	1.58	24
	0053-016	< 1.4	< 0.5	0.33	
194	0123-016A	$2.5 \pm 0.4$	$0.1 \pm .02$	0.10	10
496	0431-134	$4.8 \pm 1.1$	$0.9 \pm 0.2$	0.50	38
514	0445-205	< 2.2	< 2.0	1.00	38
	0446-205	$16.6 \pm 1.2$	$15.4 \pm 1.1$	3.16	
754	0906-094	$2.2 \pm 0.9$	$1.1 \pm 0.4$	0.25	28
1314	1131+493	$14.4 \pm 2.7$	$3.0 \pm 0.6$	5.01	18
	1132+492	$4.9 \pm 1.7$	$1.0 \pm 0.3$	0.79	
1367	1142+198	$176.2 \pm 3.6$	$15.0 \pm 0.3$	2.00	12
	1141+202B	$26.6 \pm 1.4$	$2.3 \pm 0.1$	0.03	
1656	1256+281	< 4.6	< 0.5	0.02	13
1775	1339+266B	< 0.7	< 0.6	0.79	37
1795	1346+268B	< 1.5	< 1.0	1.00	32
2142	1556+274	< 3.1	< 4.2	3.98	45
2255	1712+640	< 2.2	< 2.5	0.79	41
	1712+641	< 2.2	< 2.5	1.58	
2256	1705+786	< 1.6	< 0.7	0.16	31
	1706+786	< 1.6	< 0.7	1.00	
2589	1706+787	< 1.6	< 0.7	0.13	22
	2321+164	< 1.8	< 0.6	0.25	

<sup>a</sup> O’Dea & Owen (1985)

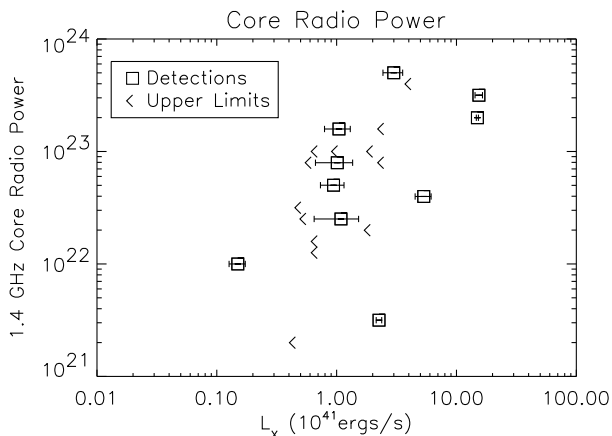


**Figure 9.** X-ray luminosity vs. 1.4GHz core radio power for NATs. The two parameters are not significantly correlated.

ters, these radio sources can now be used as an additional diagnostic for the dynamical state of clusters. The presence of a NAT located in the inner  $0.3 A_c$  of a cluster may indicate a recent or ongoing merger event.

## 5 CONCLUSIONS

We have examined the X-ray and optical properties of nearby, rich clusters of galaxies containing narrow-angle tailed radio sources. This analysis has led us to some surprising conclusions. First, clusters containing NATs show a much higher degree of substructure in their X-ray emission

than their radio-quiet counterparts. This implies clusters containing NATs are mostly dynamically complex systems, with possible recent or ongoing cluster-subcluster mergers. Also, NAT galaxies within  $0.3 A_c$  have a velocity distribution very similar to that for other radio sources, and on average below the threshold necessary to account for NAT jet bending due to ram pressure. These observations are inconsistent with the standard model for the formation of NAT radio sources, which require a high velocity galaxy traveling through the ICM to produce the ram pressure necessary to bend the radio jets backward into a U-shape. Therefore, we propose a new model for NAT formation in which NATs are, in general, galaxies with small peculiar motions existing in dynamically complex clusters which have undergone, or are undergoing, a merger with a subcluster. This merger scenario will create clusters with a high degree of substructure in their X-ray surface brightness profiles. Additionally, the ICM bulk motion caused by the merger will provide the ram pressure necessary to bend the radio jets into the NAT morphology. The ICM ram pressure will also compress and shock the ISM, possibly enhancing the compact X-ray emission detected in 40 per cent of the NATs. The luminosity and size of the compact emission observed from NATs is consistent with this mechanism. The bulk motion of the ICM may also provide the energy necessary for particle reacceleration in NAT tails, as well as additional accretion material for the central engine. This new model of radio galaxies in a violent ICM explains the observed morphological and kinematic properties of NAT galaxies and their host clusters presented in this paper.

Some additional observations could help determine if the new NAT model is correct. First, our statistics for the

correlations mentioned in this paper are low because we must rely on archival PSPC data. With the launch of the *AXAF* X-ray satellite, the sample sizes can be greatly extended. Also, higher resolution X-ray images of the X-ray bright NAT galaxies could allow us to determine the origin of the X-ray emission. At the redshifts of our sample, the *ROSAT* HRI will probe the inner 3-5 kpc of the galaxy. If the emission is still point-like, the X-rays most likely originate from the AGN. If a component of the emission is resolved, however, it must originate from some other mechanism. i.e. the galaxy ISM. We have received time in AO7 of the *ROSAT* mission to examine three NATs with the HRI. This should help constrain the X-ray emission mechanism, and provide additional insight into the formation of NAT radio sources.

## ACKNOWLEDGMENTS

We thank Jane Turner at NASA GSFC for software help. We also thank Heinz Andernach, Alistair Edge, & Chris O'Dea for useful discussions. We acknowledge NRAO for its AIPS software, NOAO for its IRAF software, and NASA GSFC for its FTOOLS and XSPEC software. This research was supported by NASA grant NAGW-3152 to J.O.B. and F.N.O., and NSF grant AST-9896039 to J.O.B.

## REFERENCES

- Abell G.O., Corwin H.G., Jr., Olowin R.P., 1989, *ApJS*, 70, 1  
 Baier F.W., 1984, *Astron. Nach.*, 305, 175  
 Balsara D.S., Norman M.L., 1992, *ApJ*, 393, 631  
 Balsara D.S., Livio M., O'Dea C.P., 1994, *ApJ*, 437, 83  
 Beers T.C., Gebhardt K., Forman W., Huchra J.P., Jones, C., 1991, *AJ*, 102, 1581  
 Begelman M.C., Rees M.J., Blandford R.D., 1979, *Nature*, 279, 770 (BRB)  
 Bernstein G.M., Nichol R.C., Tyson J.A., Ulmer M.P., Wittman, D., 1995, *AJ*, 110, 1507  
 Bird C., 1994, *AJ*, 107, 1637  
 Briel U.G., Henry J.P., 1994, *Nature*, 372, 439  
 Briel U.G., Henry J.P., 1996, *ApJ*, 472, 131  
 Briel U.G. et al., 1991, *A&A*, 246, L10  
 Brodie J.P., Bowyer S., McCarthy P., 1985, *ApJ*, 293, L59  
 Burns J.O., 1996, in Hardee P., Bridle A., Zensus A., eds, *ASP Conf. Ser. Vol. 100, Energy Transport in Radio Galaxies*. Astron. Soc. Pac., San Francisco, p. 341  
 Burns J.O., 1990, *AJ*, 99, 14  
 Burns J.O., Owen F.N., 1980, *AJ*, 85, 204  
 Burns J.O., Loken C., Gómez P., Rizza E., Bliton M., Ledlow M.J., Owen F., 1997, in Soker N., ed., *ASP Conf. Ser. Vol. 115, Galactic Cluster Cooling Flows*. Astron. Soc. Pac., San Francisco, p. 21  
 Burns J.O., Roettiger K., Pinkney J., Perley R.A., Owen F.N., Voges W., 1995, *ApJ*, 446, 583  
 Burns J.O., Rhee G., Owen F.N., Pinkney J., 1994a, *ApJ*, 423, 94  
 Burns J.O., Roettiger K., Ledlow M.J., Klypin A., 1994b, *ApJ*, 427, L87  
 Butcher H., Oemler A., 1984, *ApJ*, 285, 426  
 Butcher H., Oemler A., 1978, *ApJ*, 219, 18  
 Caldwell N., Rose J.A., Sharples R.M., Ellis R.S., Bower R.G., 1993, *AJ*, 106, 473  
 Chincarini G., Rood H.J., Sastry G.N., Welch G., 1971, *ApJ*, 168, 11  
 Colless M., Dunn A.M., 1996, *ApJ*, 458, 435  
 Couch W., Sharples R.M., 1987, *MNRAS*, 229, 423  
 Crawford C.S., Fabian A.C., 1992, *MNRAS*, 259, 265  
 David L.P., Jones C., Forman W., 1996, *ApJ*, 473, 692  
 Davis D.S., Mushotzky R.F., 1993, *AJ*, 105, 409  
 Dickey J.M., Gavazzi G., 1991, *ApJ*, 373, 347  
 Doe S.M., Ledlow M.J., Burns J.O., White R.A., 1995, *AJ*, 110, 46  
 Doi M., Fukugita M., Okamura S., Turner E.L., 1995, *AJ*, 109, 1490  
 Dressler A., Gunn J.E., 1983, *ApJ*, 270, 7  
 Dressler A., Schectman S.A., 1988, *AJ*, 95, 985  
 Eckers R.D., Fanti R., Lari C., Ulrich M.-H., 1978, *A&A*, 69, 253  
 Edge A.C., Röttgering H., 1995, *MNRAS*, 277, 1580 (ER)  
 Edge A.C., Stewart G.C., Fabian A.C., 1992, *MNRAS*, 258, 177  
 Eilek J.A., Burns J.O., O'Dea C.P., Owen F.N., 1984, *ApJ*, 278, 37  
 Fabbiano G., 1989, *ARA&A*, 27, 87  
 Fabricant D.G., Kurtz M., Geller M., Zabludoff A., Mack P., Wegner G., 1993, *AJ*, 105, 788  
 Fabricant D.G., Kent S.M., Kurtz M.J., 1989, *ApJ*, 336, 77  
 Fabricant D.G., Beers T.C., Geller M.H., Gorenstein P., Huchra J.P., Kurtz M.J., 1986, *ApJ*, 308, 530  
 Feretti L., Böehreinger H., Giovannini G., Neumann D., 1997, *A&A*, 317, 432  
 Feretti L., Perola G.C., Fanti R., 1992, *A&A*, 265, 9  
 Fitchett M.J., Webster R., 1987, *ApJ*, 317, 653  
 Flin P., Trevese D., Cirimele G., Hickson P., 1995, *A&AS*, 110, 313  
 Gavazzi G., Randone I., Branchini E., 1995, *ApJ*, 438, 590  
 Gavazzi G., Contursi A., Carrasco L., Boselli A., Kennicutt R., Scodreggio M., Jaffe W., 1995, *A&A*, 304, 325  
 Geller M.J., Beers T.C., 1982, *PASP*, 94, 421  
 Girardi M., Escalera E., Fadda D., Giuricin G., Mardirossian F., Mezzetti M., 1997, *ApJ*, 482, 41  
 Gómez P.L., Pinkney J., Burns J.O., Wang Q., Owen F.N., Voges W., 1997, *ApJ*, 474, 580  
 Grebenev S.A., Forman W., Jones C., Murray S., 1995, *ApJ*, 445, 607  
 Hanisch R.J., 1982, *A&A*, 116, 137  
 Hatsukade I., 1990, PhD thesis, Osaka Univ.  
 Havlicek L.L., Crain R.D., 1988, *Practical Statistics for the Physical Sciences*, Amer. Chem. Soc., Washington, DC  
 Henriksen M.J., 1993, *ApJ*, 414, L5  
 Henriksen M.J., Markevitch M., 1996, *ApJ*, 466, 79  
 Henry J.P., Briel, U.G. 1996, *ApJ*, 472, 137  
 Hintzen P., 1979, *PASP*, 91, 426  
 Ishii T., Matsuda T., Shima E., Livio M., Anzer U., Boerner G., 1993, *ApJ*, 404, 706  
 Isobe T., Feigelson E.D., Nelson P.I., 1986, *ApJ*, 306, 490  
 Jaffe W.J., Rudnick L., 1979, *ApJ*, 233, 453  
 Jedrzejewski R.I., 1987, *MNRAS*, 226, 747  
 Jenner D.C., 1974, *ApJ*, 191, 55  
 Jones C., Forman W., 1984, *ApJ*, 276, 38  
 Jones T.W., Owen F.N., 1979, *ApJ*, 234, 818 (JO)  
 Kriessler J.R., Beers T.C., 1997, *AJ*, 113, 80  
 La Valley M., Isobe T., Feigelson E.D., 1992 in Worrall D.M., Biemesderfer C., Barnes J., eds, *ASP Conf. Ser. Vol. 25, Astronomical Data Analysis Software and Systems I*. Astron. Soc. Pac., San Francisco, p. 245  
 Ledlow M.J., Owen F.N., 1996, *AJ*, 112, 9  
 Ledlow M.J., Owen F.N., 1995, *AJ*, 109, 853  
 Lima Neto G.B., Pislak V., Durret F., Gerbal D., Slezak E., 1997, *A&A*, 327, 81  
 Loken C., Roettiger K., Burns J.O., Norman M.L., 1995, *ApJ*, 445, 80  
 Loken C., Burns J.O., Norman M.L., Clarke D.A., 1993, *ApJ*, 417, 515

- Mack K.H., Feretti L., Giovannini G., Klein U., 1993, *A&A*, 280, 63
- Mackie G., 1992, *ApJ*, 400, 65
- McNamara B.R., Wise M., Sarazin C., Jannuzi B.T., Elston R., 1996a, *ApJ*, 466, L9
- McNamara B.R., Jannuzi B.T., Elston R., Sarazin C.L., Wise M., 1996b, *ApJ*, 469, 66
- Malumuth E.M., Kriss G.A., Dixon W.V., Ferguson H.C., Ritchie C., 1992, *AJ*, 104, 495
- Markevitch M., 1996, *ApJ*, 465, L1
- Mazure A., Gerbal D., Proust D., Capelato H.V., 1986, *A&A*, 157, 159
- Mellier Y., Mathez G., Mazure A., Chauvineau B., Proust D., 1988, *A&A*, 199, 67
- Minkowski R., 1958, *PASP*, 70, 143
- Miyaji, T. et al., 1993, *ApJ*, 419, 66
- Mohr J.J., Fabricant D.G., Geller M.J., 1993, *ApJ*, 413, 492
- O'Dea C.P., 1985, *ApJ*, 295, 80
- O'Dea C.P., Owen F.N., 1985, *AJ*, 90, 954
- O'Dea C.P., Sarazin C.L., Owen F.N., 1987, *ApJ*, 316, 113
- O'Donoghue A.A., Eilek J.A., Owen F.N., 1993, *ApJ*, 408, 428
- Oegerle W.R., Fitchett M.J., Hoessel J.G., 1989, *AJ*, 97, 627
- Oegerle W.R., Hill J.M., Fitchett M.J., 1995, *AJ*, 110, 32
- Owen F.N., Ledlow M.J., 1997, *ApJS*, 108, 41
- Owen F.N., Ledlow M.J., Keel, W.C., 1995, *AJ*, 109, 14
- Pinkney J.P., et al., 1996, *ApJ*, 468, L13
- Prestwich A.H., Guimond S.J., Luginbuhl C.B., Joy M., 1995, *ApJ*, 438, L71
- Raymond J.C., Smith B.W., 1977, *ApJS*, 35, 419
- Roettiger K., Stone J.M., Mushotzky R.F., 1998, *ApJ*, 493, 62
- Roettiger K., Burns J.O., Loken C., 1996, *ApJ*, 473, 651
- Roettiger K., Burns J.O., Pinkney J., 1995, *ApJ*, 453, 634
- Roettiger K., Burns J.O., Loken C., 1993, *ApJ*, 407, L53
- Rood J.H., Sastry G.N., 1971, *PASP*, 83, 313
- Röttgering H., Snellen I., Miley G., DeJong J.P., Hanisch R.J., Perley R., 1994, *ApJ*, 436, 654
- Ruffert M., Arnett D., 1994, *ApJ*, 427, 351
- Schindler S., Müller, E., 1993, *A&A*, 272, 137
- Simon A.B., 1979, *MNRAS*, 188, 637
- Slee O.B., Reynolds J.E., 1984, *PASAu*, 5, 516
- Slezak K.E., Durrett F., Gerbal D., 1994, *AJ*, 108, 1996
- Smith E.P., Bohlin R.C., Bothun G.D., O'Connell R.W., Roberts M.S., Neff S.G., Smith A.M., Stecher T.P., 1997, *ApJ*, 478, 516
- Stauffer J., Spinrad H., Sargent W.L.W., 1979, *ApJ*, 228, 379
- Struble M.F., Rood H.J., 1991, *ApJS*, 77, 363
- Tarengi M., Scott J.S., 1976, *ApJ*, 207, L9
- Trevese D., Flin P., Migliori L., Hickson P., Pittella G., 1992, *A&AS*, 94, 327
- Vallée J.P., Roger R.S., 1987, *AJ*, 94, 1
- Vallée J.P., Wilson A.S., 1976, *Nature*, 259, 451
- Van Breugel W., Filippenko A.V., Heckman T., Miley G., 1985, *ApJ*, 293, 83
- Venkatesan T.C.A., Batuski D.J., Hanisch R.J., Burns J.O., 1994, *ApJ*, 436, 67
- Vikhlinin A., Forman W., Jones C., 1997, *ApJ*, 474, L7
- West M.J., Bothun D., 1990, *ApJ*, 350, 36
- White R.E. III, Day C.S.R., Hatsukade I., Hughes J.P., 1994, *ApJ*, 433, 583
- Wilson A.S., Vallée J.P., 1977, *A&A*, 58, 79
- Zabludoff A.I., Franx M., Geller M.J., 1993, *ApJ*, 419, 47
- Zabludoff A.I., Geller M.J., Huchra J.P., Vogeley M.S., 1993, *AJ*, 106, 273

## 6 APPENDIX: INDIVIDUAL SOURCES

**Abell 85:** *Fig. 1a.* This strong cooling flow cluster has received much attention over the past few years in both the optical and X-ray. Analysis of the optical properties of this cluster yield a virial mass of  $\approx 9 \times 10^{14} M_{\odot}$  and no obvious evidence of substructure (Girardi et al. 1997; Malumuth et al. 1992). However, the cD galaxy does have a large peculiar velocity of  $390 \text{ km s}^{-1}$  with respect to the cluster mean velocity. The X-ray emission near the cD appears to be inhomogeneous, with several clumps of X-ray enhancement which do not seem to be associated with any faint galaxies in the optical (Prestwich et al. 1995). The southern-most NAT in the cluster is associated with a clump of X-ray emission within  $\approx 100 \text{ kpc}$  of the host radio galaxy. This subclump may be the signature of a possible accretion event. Lima Neto et al. (1997) agree that the southern X-ray extension contains a diffuse X-ray component in addition to X-rays from individual galaxies. High resolution radio images (O'Dea & Owen 1985) reveal that the radio source to the NE of the cluster centre is also a NAT, although we do not see excess X-ray emission associated with this source.

**Abell 119:** *Fig. 1b.* This cluster shows the best example of NAT tails aligning with the asymmetric cluster X-ray emission. Both NATs are pointing directly toward the NE elongation of the cluster. *HEAO 1 A2* spectral observations of A119 detected possible nonisothermal emission from this cluster, which may be evidence for a merger event (Henriksen 1993; Roettiger, Burns & Pinkney 1995). *Einstein* IPC and HRI data also support the idea of substructure in the X-ray morphology of the cluster, which closely maps the asymmetric galaxy distribution (Fabricant et al. 1993). However, examination of the optical position and velocity data for the galaxies in A119 show no evidence of substructure (Girardi et al. 1997; Kriessler & Beers 1997; West & Bothun 1990). Polarization studies of these two NATs show the magnetic fields to be oriented along the jet, with high polarization in 0053-015, and much lower polarization in 0053-016 (Mack, et al. 1993).

**Abell 194:** *Fig. 1c.* The striking feature in the X-ray emission from this cluster is the strong elongation to the NW/SE, where a similar feature is found in the galaxy distribution. Some galaxy position and velocity analyses do not show evidence of substructure (Girardi et al. 1997; West & Bothun 1990), while an adaptive kernel analysis of the galaxy positions indicate the presence of substructure (Kriessler & Beers 1997). Although the radio map of this cluster is dominated by a twin jet to the NE, the NAT of interest is the radio source near the centre of this map. This cluster is also the location of Minkowski's Object (Minkowski 1958), which is located coincident with the NAT radio jet. It is suggested to be a cloud of gas imbedded in the radio jet, which is now experiencing a burst of star formation (Brodie, Bowyer & McCarthy 1985; Van Breugel et al. 1985).

**Abell 496:** *Fig. 1d.* This cooling flow cluster contains a NAT in the SE coincident with a compact X-ray source. The X-ray emission near the cD galaxy in this cluster exhibits inhomogeneities that may be associated with cooling flow filaments (Prestwich et al. 1995). As further evidence of a cooling flow, the emission line nebula found at the centre of the cooling flow is attributed to thin layers of self-absorbing

gas around the surfaces of cold clouds embedded in the hot, X-ray emitting gas (Crawford & Fabian 1992). Additionally, there is strong evidence for centrally enhanced metal abundance from data gathered by the *Ginga* LAC and *Einstein* SSS detectors (White et al. 1994). A central cooling time of  $T_{\text{cool}} \approx 2.1 \pm 0.3$  Gyr, and a mass inflow rate,  $\dot{M} \sim 112 M_{\odot} \text{ yr}^{-1}$  have been calculated (Edge, Stewart & Fabian 1992). Malumuth et al. (1992) conclude that this cluster does not show substructure in its galaxy velocity distribution, and calculate a virial mass of  $\approx 7 \times 10^{14} M_{\odot}$ . However, other work (Kriessler & Beers 1997; Mazure et al. 1986) detects structure in the galaxy distribution, which is mimicked in the slight elongation of the core X-ray emission to the south, and the slight NW elongation of the outer X-ray emission.

**Abell 514:** *Fig. 1e.* This cluster possesses very clumpy, asymmetric X-ray emission, with a large centroid shift in its elliptical isophotes. The two NATs are each associated with X-ray subclumps in the cluster emission.

**Abell 1775:** *Fig. 1f.* The NAT in this cluster has its core emission near the X-ray peak. The tail extends in a direction coincident with an X-ray enhancement to the NE of the X-ray centre. This X-ray elongation is offset from the galaxy distribution which is oriented mainly E-W (Trevese et al. 1992). Galaxy velocity data show this cluster to perhaps be two poor, interacting clusters, separated by  $\sim 3000 \text{ km s}^{-1}$  (Oegerle, Hill & Fitchett 1995). The NAT galaxy was once thought to be part of a bound binary galaxy pair (Jenner 1974). The measured velocity difference of these two galaxies is  $\approx 1700 \text{ km s}^{-1}$ , and therefore, the galaxies were assumed to be supermassive ( $M > 2 \times 10^{13} M_{\odot}$ ) in order for them to be bound (Chincarini et al. 1971). However, the measured dispersion of A1775 ( $1594 \text{ km s}^{-1}$ , Struble & Rood 1991), allows for these galaxies to be unbound, and therefore of average mass (Hintzen 1979).

**Abell 754:** *Fig. 1g.* A754 is an excellent example of a cluster which has undergone a merger. Henriksen & Markevitch (1996) found strong evidence for temperature structure in this cluster which supports the earlier findings of Henry & Briel (1996). The area to the NW of the cluster centre shows temperatures in excess of 12 keV, while a cooler component below 5 keV is present to the SE. The elongation of the cluster X-ray centre may be due to an off-axis merger of two subclusters (Roettiger, Stone & Mushotzky 1998; Henriksen & Markevitch 1996). The optical data are less conclusive, with some studies showing evidence both for (Girardi et al. 1997; Kriessler & Beers 1997; West & Bothun 1990; Dressler & Schectman 1988) and against (Geller & Beers 1982; Fabricant et al. 1986; Bird 1994) the presence of substructure. This cluster exhibits an extreme centroid shift and change in ellipticity in our analysis. The NAT is a very small radio source that was often mistaken for compact emission, until viewed at high resolution. Another NAT is coincident with the knot of X-ray emission to the SW of the cluster, but its location beyond  $0.3 A_c$  placed it outside our sample selection criteria.

**Abell 1314:** *Fig. 1h.* This cluster shows very clumpy, elongated X-ray emission, and a strong X-ray centroid shift. This elongation is also present in the galaxy distribution, which shows a definite ellipticity, and is oriented mainly E-W (Flin et al. 1995). The cluster contains two narrow-angle tailed radio sources with the western NAT's tail di-

rection aligned with the local X-ray emission. Although not detectable here, the NAT to the east (IC711) has one of the longest tails ever detected, extending 17 arcmin (630 kpc) at a wavelength of 74 cm (Vallée & Roger 1987).

**Abell 1367:** *Fig. 1i.* This cluster contains the strong X-ray and radio source 3C264, located in the SW corner of the cluster. A second NAT in the NW has often been misclassified as a double radio source at low resolution. Grebenev et al. (1995) performed a wavelet analysis of the *ROSAT* PSPC and *Einstein* HRI images of this cluster, and found sixteen extended X-ray features—nine of which had galaxies coincident. This elongated NW region also contains several spiral galaxies that appear to be infalling for the first time. HI maps of these spirals show the neutral hydrogen emission to be offset from the optical centres and asymmetric in shape, implying the galaxy discs are interacting with the ICM (Dickey & Gavazzi 1991). As further evidence for ram pressure induced star formation, these spiral galaxies all show giant HII regions aligned along a peripheral path, suggestive of a bow shock formation mechanism (Gavazzi et al. 1995). The luminosity function of spiral galaxies in this cluster deviates from that of field spirals at the faint end, with bluer spirals existing in the cluster. This is another indication of galaxy-ICM interactions causing enhanced star formation activity (Gavazzi, Randone, & Branchini 1995).

**Abell 1656:** *Fig. 1j.* The very rich Coma cluster has only one NAT associated with it. The tail of the NAT is oriented in a direction similar to the core elongation. It is believed that Coma has recently undergone a cluster/subcluster merger (Burns et al. 1994b). This has been confirmed by several optical studies (Baier 1984; Fitchett & Webster 1987; Mellier et al. 1988; Colless & Dunn 1996; Zabludoff, Franx, & Geller 1993; Caldwell et al. 1993); however, the optical state of this cluster is still poorly understood (e.g. Geller & Beers 1982; Dressler & Schectman 1988; West & Bothun 1990). The merger hypothesis is supported by filamentary X-ray emission in the E and SE detected through a wavelet analysis (Vikhlinin, Forman & Jones 1997), and smaller X-ray subclumps detected by the *Einstein* IPC (Davis & Mushotzky 1993). The galaxy distribution in Coma is also peculiar, with the majority of early-type galaxies lying along a filament to the NE/SW direction, while the late-type galaxies are more symmetrically distributed (Doi et al. 1995). The luminosity function in the core of Coma is well fit by a power law with slope  $-1.42 \pm 0.05$  over the range  $-19.4 < M_R < -11.4$  (Bernstein et al. 1995). Caldwell et al. (1993) detected a number of “E+A” (Dressler & Gunn 1983) galaxies, which are almost exclusively located to the SW of the cluster centre. This is a surprising result since most of these post-starburst galaxies are detected in distant ( $z \sim 0.2$ ) clusters (Butcher & Oemler 1978, 1984; Dressler & Gunn 1983; Couch & Sharples 1987).

**Abell 1795:** *Fig. 1k.* This cooling flow cluster shows asymmetry in its galaxy distribution (Oegerle, Fitchett, & Hoessel 1989). However, combined with velocity information, no optical substructure is present (Girardi et al. 1997). The northern galaxy elongation is mimicked by the X-ray emission which also shows an excess to the north of the cluster core (Briel & Henry 1996). The cooling flow is evidenced by a cooler temperature component to the X-ray emission (Briel & Henry 1996; White et al. 1994), with  $T_{\text{cool}} \approx 2.1 \pm 0.3$  Gyr, and  $\dot{M} \sim 478 M_{\odot} \text{ yr}^{-1}$  (Edge et

al. 1992). Recently, attention has been focused on *HST* examination of the cD galaxy. This galaxy shows excess H $\alpha$  and UV filaments, as well as a dust lane coincident with the edges of the radio lobes (Pinkney et al. 1996; McNamara et al. 1996a, 1996b), which may imply massive star formation in a cooling flow (Smith et al. 1997).

**Abell 2255:** *Fig. 1l.* Multiwavelength studies indicate A2255 to be a likely merger candidate (Burns et al. 1995). The velocity data for this cluster can either support (Tarengi & Scott 1976) or refute (Stauffer, Spinrad & Sargent 1979) the merger hypothesis. The X-ray data show an elongation in the E-W direction, and possible multiple temperature components (Feretti et al. 1997). Additionally, Jones & Forman (1984) measured a very large core radius for this cluster ( $\approx 0.4$  Mpc). A2255 contains a radio halo source (Jaffe & Rudnick 1979; Hanisch 1982), which may be produced as a merger byproduct (Burns 1996) or by particle reacceleration by the multiple NAT tails (Feretti et al. 1997).

**Abell 2142:** *Fig. 1m.* This cooling flow cluster has a clear elongation in its X-ray emission to the NE/SW, with the NAT oriented in roughly the same direction. The cooling flow manifests itself in a cool component fit to the X-ray spectrum, as well as strong evidence for a centrally enhanced metal abundance (White et al. 1994). A2142 has a cooling time of  $3.0 \pm 0.8$  Gyr, and a mass inflow rate  $\sim 188 M_{\odot} \text{ yr}^{-1}$  (Edge et al. 1992). X-ray surface brightness and temperature maps imply A2142 is in the late stages of a merger (Henry & Briel 1996). This cluster also has a high velocity dispersion of  $1280 \text{ km s}^{-1}$  (Oegerle et al. 1995). The X-ray point source in the NE is most likely associated with a Seyfert 1 cluster member galaxy.

**Abell 2589:** *Fig. 1n.* This cooling flow cluster shows an obvious elongation to the N/S in the X-ray although the gas appears to be isothermal (David, Jones & Forman 1996). There is also an enhancement of emission to the south, near the NAT. Optical data analysed by Beers et al. (1991) found evidence for substructure. They also note that A2589 and the nearby cluster A2593 form a bound pair. The envelope of the cD galaxy shows no evidence of a colour gradient, which is consistent with the envelope being produced by mergers (Mackie 1992).

**Abell 2256:** *Fig. 1o.* This cluster is one of the best examples of clusters containing temperature substructure in the X-ray emitting gas (Briel & Henry 1994). A wavelet analysis (Slezak, Durrett & Gerbal 1994), as well as isophotal analysis (Davis & Mushotzky 1993) of the X-ray emission shows extreme X-ray substructure, in accord with the large centroid shift detected in this analysis. The X-ray emission from A2256 shows two distinct peaks, which has been interpreted as the main cluster peak along with a smaller subcluster in the process of merging (Briel et al. 1991; Roettiger et al. 1995). The main cluster has a temperature of 7.5 keV (Hatsukade 1990), while the subcluster has a temperature ranging from 2 keV (Hatsukade 1990) to 4.6 keV (Miyaji et al. 1993) to 6.2 keV (Markevitch 1996). From *BBXRT* and *ROSAT* data, Miyaji et al. (1993) calculate a gravitational mass of  $\sim 2.8 - 3.7 \times 10^{14} M_{\odot}$ . The galaxy density field appears to be elliptical, and elongated in the same direction as the cluster gas (Fabricant, Kent, & Kurtz 1989). This cluster also contains a radio halo source, several NAT sources, and a steep spectrum radio source. The halo source may ac-

tually be several NAT galaxies which are distorted due to the subcluster merger (Röttgering et al. 1994).

This figure "fig1a.gif" is available in "gif" format from:

<http://arxiv.org/ps/astro-ph/9811005v1>



This figure "fig1b.gif" is available in "gif" format from:

<http://arxiv.org/ps/astro-ph/9811005v1>

This figure "fig1c.gif" is available in "gif" format from:

<http://arxiv.org/ps/astro-ph/9811005v1>

This figure "fig1d.gif" is available in "gif" format from:

<http://arxiv.org/ps/astro-ph/9811005v1>